Kinetic Study of the Reactions of Gas Phase Pd(a^1S_0), Ag($5s\ ^2S_{1/2}$), Au($6s\ ^2S_{1/2}$), Cd($5s^2\ ^1S_0$), and Hg($6s^2\ ^1S_0$) Atoms with Nitrous Oxide

Mark L. Campbell†

Chemistry Department, United States Naval Academy, Annapolis, Maryland 21402

Received: August 27, 2002; In Final Form: February 26, 2003

The reactivity of gas-phase Pd(a^1S_0), Ag($5s\ ^2S_{1/2}$), Au($6s\ ^2S_{1/2}$), Cd($5s^2\ ^1S_0$), and Hg($6s^2\ ^1S_0$) with N_2O as a function of temperature and pressure is reported. The transition metal atoms were produced by the photodissociation of an appropriate precursor molecule and detected by laser-induced fluorescence. The reaction of palladium with N_2O is pressure dependent indicating adduct formation. The room-temperature limiting low-pressure third-order rate constant is $(2.5 \pm 0.8) \times 10^{-30}$ molecule^{-2} cm^6 s^{-1} in argon buffer. The limiting low-pressure third-order rate constant can be expressed as $\log k_0(T) = -219.06 + 152(\log T) - 30.5(\log T)^2$ molecule^{-2} cm^6 s^{-1} over the temperature range 294−523 K. The reactions of ground-state silver, gold, cadmium, and mercury with N_2O are very slow, and only upper limits for the rate constants can be reported for these reactions.

Introduction

The reactions of gas-phase metal atoms with nitrous oxide have recently received considerable attention because of a number of both fundamental and practical reasons.[1,2] The reactions of transition metal atoms, TM, with N_2O

$$TM(g) + N_2O(g) \rightarrow TMO(g) + N_2(g) \qquad (1)$$

are all exothermic[3,4] because of the formation of the stable N_2 and metal oxide molecules. Despite this exothermicity, metal atom reactions with N_2O have been observed to have significant energy barriers. These barriers have been attributed to the requirement of a nonadiabatic transition along the reaction pathway.[5]

Transition metal chemistry is an intriguing field of study because of the high multiplicities of the atomic ground states and the large number of low-lying metastable states. For many TM atoms, states resulting from s^2d^{n-2} and s^1d^{n-1} configurations (where n refers to the number of valence electrons) are nearly degenerate so the electronic structure of the atom plays an important role in its reaction dynamics. The kinetics of the transition metals reacting with N_2O have previously received considerable attention.[6−33] Here, we report the kinetics of the remainder of the nonradioactive transition metals reacting with N_2O. With the completion of this study, rate constants for the reactions of all of the transition metals with the exception of Tc have now been reported.

Experimental Section

Kinetic experiments in our laboratory utilize pseudo-first-order conditions ([TM] ≪ [N_2O]) in an apparatus with slowly flowing gas. The experimental apparatus and technique have been described in detail elsewhere.[34] Briefly, the reaction chamber is a stainless steel reducing 4-way cross with attached sidearms and a sapphire window for optical viewing. The reaction chamber is enclosed within a convection oven (Blue M, model 206F, $T_{max} = 623$ K) with holes drilled to allow for the exiting sidearms and the telescoping of the LIF signal to the PMT.

Transition metal atoms are produced by the 248 nm photodissociation of the appropriate precursor with the output of an excimer laser (Lambda Physics Lextra 200). Some precursors require the focusing of the beam to observe the atomic signal. When focusing is required, a lens ($f = 564$ mm) is placed approximately one focal length from the reaction zone. The preferred arrangement is without a focusing lens because focusing tends to produce a greater percentage of excited state atoms. Transition metal atoms are detected via LIF using an excimer-pumped dye laser (Lambda Physics Lextra 50/Scan-Mate 2E). The fluorescence is detected at 90° to the counter-propagated laser beams with a three-lens telescope imaged through an iris. Interference filters are used to isolate the LIF. A photomultiplier tube (Hamamatsu R375) is used in collecting the LIF which is subsequently sent to a gated boxcar sampling module (Stanford Research Systems SR250), and the digitized output is stored and analyzed by a computer.

The transition metal precursor is entrained in a flow of buffer gas. The diluted precursor, buffer gas, and N_2O flow through calibrated mass flow meters and flow controllers prior to admission to the reaction chamber. Each sidearm window is purged with a slow flow of buffer gas to prevent deposition of metal atoms and other photoproducts. Pressures are measured with MKS Baratron manometers, and chamber temperatures are measured with a thermocouple.

The delay time between the photolysis pulse and the dye-laser pulse is varied by a digital delay generator (Stanford Research Systems DG535) controlled by a computer interfaced through a Stanford Research Systems SR245 computer interface. The trigger source for these experiments is scattered pump laser light incident upon a fast photodiode. LIF decay traces typically consist of 200 data points, each point averaged from 3 to 5 laser shots.

† Henry Dreyfus Teacher-Scholar.

10.1021/jp021957m
Published on Web 04/08/2003

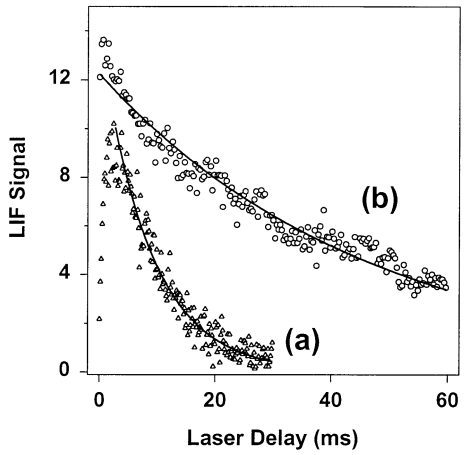

Figure 1. Typical decay curves with added N_2O in N_2 buffer at 623 K: (a) Au($a^2S_{1/2}$), $P_{total} = 100.0$ Torr, $P(N_2O) = 27.9$ Torr, $\tau = 8.6$ ms; (b) Cd(a^1S_0), $P_{total} = 100.0$ Torr, $P(N_2O) = 93.8$ Torr; $\tau = 48$ ms. The solid lines through the data are least-squares fits.

Data Analysis and Results

Under pseudo-first-order conditions in which no production processes occur after the initial photolysis event, the decrease in the [TM] with time following the photolysis laser pulse is given by

$$-\mathrm{d[TM]}/\mathrm{d}t = (k_{obs}[N_2O] + k_d)[TM] = (1/\tau)[TM] \quad (2)$$

where k_{obs} is the observed second-order rate constant due to N_2O at fixed buffer gas pressure, k_d represents the depletion rate constant due to the reaction of transition metal with precursor molecules and fragments and diffusion out of the detection zone, and τ is the observed time constant for transition metal depletion in the presence of a given [N_2O], precursor, and buffer gas pressure. The LIF signal at time t after photolysis is proportional to [TM]. Thus

$$\mathrm{LIF} = \mathrm{LIF}_0 \exp(-t/\tau) \quad (3)$$

where LIF_0 is the initial LIF signal immediately following the photolysis laser pulse. LIF decays which exhibit single-exponential behavior are fitted using a least-squares procedure to determine τ. The decays for silver, cadmium, and mercury exhibited single-exponential behavior. Plot b in Figure 1 illustrates the exponential behavior exhibited by cadmium.

As a result of the photolysis of the transition metal precursor, atoms in excited states are often produced in significant quantities. These excited state atoms possibly complicate the temporal profile of the ground state. For a ground state in which quenching of excited states after the initial photolysis laser pulse is important, the time dependence of the ground state's concentration will exhibit biexponential behavior. If this situation is not handled properly, significant errors in the determination of the values of the rate constants can occur. For cases where the decay rate of an excited state down to the ground state is fast compared to the removal rate of the ground state, cascade processes are unimportant at long times, and the ground-state removal rate is determined by analysis of the decay at long times. Biexponential behavior of this type has been observed for numerous transition metals.[21−24,27,28,33] Figures 1a and 2 illustrate this type of behavior which was observed for gold and palladium, respectively. When analyzing data with a biexponential component, it is critical that the time constant does not include contributions from the growth due to decay of

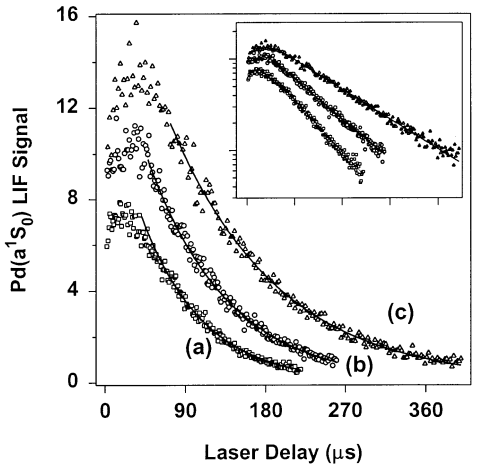

Figure 2. Typical Pd(a^1S_0) decay curves with added N_2O in argon buffer at 294 K and $P_{total} = 20.0$ Torr: (a) $P(N_2O) = 0.559$ Torr, $\tau = 69$ μs; (b) $P(N_2O) = 0.420$ Torr; $\tau = 89$ μs; (c) $P(N_2O) = 0.280$ Torr, $\tau = 120$ μs. The solid lines through the data are least-squares fits. The inset is a ln plot of the data.

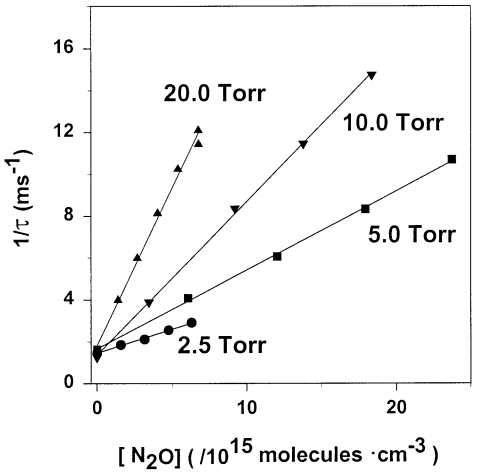

Figure 3. Typical plots for determining k_{obs} for Pd(a^1S_0) + N_2O at 294 K. The solid line for each set of data is a linear regression fit from which k_{obs} is obtained.

excited states. In Figures 1a and 2, the solid lines indicate the range of data used to calculate the value of the time constant.

Once the reaction time constant has been determined for a series of nitrous oxide concentrations, the slope of a plot of $1/\tau$ vs [N_2O] yields the observed second-order rate constant, k_{obs}. Figures 3 and 4 illustrate examples of these types of plots for palladium. The relative uncertainty (i.e., the reproducibility) of the second-order rate constants is estimated at ±20% based on repeated measurements of rate constants under identical temperature and total pressure conditions. The absolute uncertainties are conservatively estimated to be ±30% and are based on the sum of the statistical scatter in the data, uncertainty in the flowmeter and flow controller readings (5%) and the total pressure reading (1%), uncertainties due to incomplete gas mixing, and uncertainties due to incomplete relaxation of the excited electronic states to the ground state.

Many of the reactions of transition metal atoms with nitrous oxide are very slow. In some cases, the rates are slower than the detection limit of our experimental method. For our experimental arrangement, the detection limit for the measurement of rate constants depends on the transition metal being studied. This variation in the detection limit as a function of transition metal atom is due to two factors: (1) the conditions

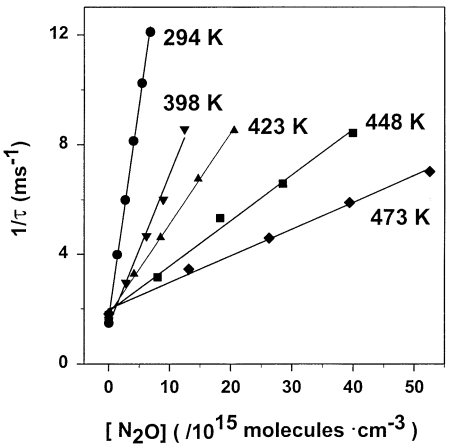

Figure 4. Typical plots for determining k_{second} as a function of temperature for Pd(a^1S_0) + N_2O at 20.0 Torr. The solid line for each set of data is a linear regression fit from which k_{obs} is obtained.

TABLE 1: Second-Order Rate Constants[a] and Limiting Low-Pressure Third-Order Rate Constants for Pd(a^1S_0) Reacting with N_2O

temp (K)	pressure (Torr)	k_{obs} (10^{-13} molecule^{-1} cm^3 s^{-1})	k_0 (10^{-31} molecule^{-2} cm^6 s^{-1})
294[b]	2.5	2.3	25.
	5.0	3.8	
	10.0	7.4	
	15.0	11.	
	20.0	16.	
348	10.0	5.0	17.
	20.0	9.4	
373	10.0	4.1	15.
	20.0	7.9	
398	20.0	5.6	12.
423	20.0	3.3	7.2
448	20.0	1.7	3.9
473	20.0	0.98	2.4
498	20.0	0.41	1.1
523	20.0	0.24	0.65

[a] Absolute uncertainties are estimated at ±30%. [b] Room-temperature varied from 293 to 295 K.

necessary to attain a measurable LIF signal and (2) the lifetime of the transition metal in the detection zone in the absence of oxidant. The factors affecting our detection limit have been described in detail elsewhere,[33] and the same arguments apply for these experiments. For the transition metals reported here, all but palladium exhibited reaction rates too slow at the temperatures studied such that the rate constants are smaller than the detection limit of our system; therefore, for these atoms, only upper limits for the rate constants could be determined at these temperatures.

Pd(a^1S_0). Pressure and temperature-dependent rate constants were measured utilizing $Pd(CF_3CO_2)_2$ as a precursor. Detection of palladium atoms was accomplished by exciting the 5p $^3D_1°$−a^1S_0 transition at 247.642 nm and detecting the 5p $^3D_1°$−5s $^1D_2$ transition at 348.977 nm. A broadband interference filter centered at 350 nm was utilized to isolate the fluorescence. Second-order rate constants in argon buffer as a function of temperature and pressure are listed in Table 1. The reaction of palladium with N_2O is pressure dependent indicating adduct formation. The measured rate constants at 294, 348, and 373 K measured at pressures of 20 Torr and below fell within the linear third-order regime. The calculated limiting low-pressure third-order rate constants are listed in Table 1. Rate constants above 373 K were only measured at 20 Torr and are expected to be in the linear regime as the linear regime is expected to extend to higher pressures at higher temperatures. The reaction of palladium with O_2 remained in the linear regime well past 100 Torr total pressure.[35] We were unable to measure rate constants in the falloff region because of signal detection problems at the high pressures required. The third-order rate constants decrease dramatically with increasing temperature. The limiting low-pressure third-order rate constants are fit by the expression

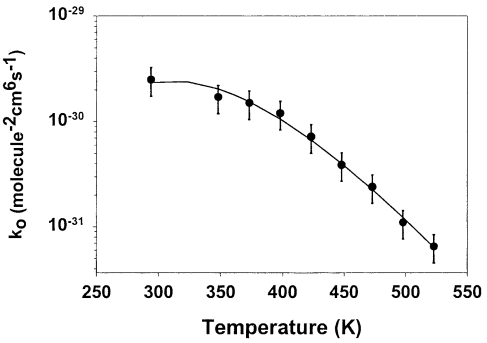

Figure 5. Temperature dependence of the limiting low-pressure third-order rate constant k_0. The solid line is a polynomial fit in log T. See text for the results of the fit.

$$\log k_0(T) = -219.06 + 152(\log T) - 30.5(\log T)^2 \text{ molecule}^{-2}\text{ cm}^6\text{ s}^{-1} \quad (4)$$

over the temperature range 294−523 K. The experimental data and a fit to the data using eq 4 are shown in Figure 5.

Ag(5s $^2S_{1/2}$). Rate constant measurements were attempted up to a temperature of 623 K in N_2 buffer utilizing $Ag(CF_3COCHCOCF_3)P(CH_3)_3$ as precursor. Detection of silver atoms was accomplished by both exciting and detecting the fluorescence from the 5p $^2P_{1/2}°$−5s $^2S_{1/2}$ transition at 338.289 nm. A UG-1 filter was utilized to isolate the fluorescence. The rate of this reaction is extremely slow so that we can only report an upper limit. Detection of silver atoms could be observed at 623 K in partial pressures of N_2O up to 26 Torr. The lifetime of silver under these conditions was approximately 1400 μs. Based on these data, we report an upper limit for the reaction of Ag($^2S_{1/2}$) at 623 K of 2×10^{-15} molecule^{-1} cm^3 s^{-1}. Assuming a preexponential factor of approximately the gas kinetic collision rate, we can place a lower limit on the activation energy of approximately 60 kJ/mol.

Au(6s $^2S_{1/2}$). Temperature-dependent rate constant measurements were attempted up to a temperature of 623 K in N_2 buffer utilizing $(CH_3)_2(C_5H_7O_2)Au$ as a precursor. Detection of gold atoms was accomplished by exciting the 6p $^2P_{3/2}°$−6s $^2S_{1/2}$ transition at 242.795 nm and detecting the 6p $^2P_{3/2}°$−6s^2 $^2D_{5/2}$ transition at 312.278 nm. A broadband interference filter centered at 300 nm was utilized to isolate the fluorescence. The rate of this reaction is extremely slow so that we can only report an upper limit. Detection of gold atoms could be observed at 623 K in partial pressures of N_2O up to 27.9 Torr. The lifetime of gold under these conditions was approximately 8600 μs. Based on these data, we report an upper limit for the reaction of Au($^2S_{1/2}$) at 623 K of 3×10^{-16} molecule^{-1} cm^3 s^{-1}. Assuming a preexponential factor of approximately the gas kinetic collision rate, we can place a lower limit on the activation energy of approximately 70 kJ/mol.

Cd(5s^2 $^1S_0$). Temperature-dependent rate constant measurements were attempted up to a temperature of 623 K in N_2 buffer utilizing $Cd(acac)_2$ as a precursor. Detection of cadmium atoms was accomplished by both exciting and detecting the fluorescence from the 5p $^1P_1°$−5s^2 $^1S_0$ transition at 228.802 nm. A

narrowband interference filter centered at 228 nm was utilized to isolate the fluorescence. The rate of this reaction is extremely slow so that we can only report an upper limit. Detection of cadmium atoms could be observed at 623 K in partial pressures of N_2O up to 93.8 Torr. The lifetime of cadmium under these conditions was approximately 48 ms. Based on these data, we report an upper limit for the reaction of $Cd(5s^2\ ^1S_0)$ at 623 K of 2×10^{-17} molecule^{-1} cm^3 s^{-1}. Assuming a preexponential factor of approximately the gas kinetic collision rate, we can place a lower limit on the activation energy of approximately 80 kJ/mol.

$Hg(6s^2\ ^1S_0)$. Temperature-dependent rate constant measurements were attempted up to a temperature of 423 K in N_2 buffer utilizing $Hg(CH_3)_2$ as a precursor. Detection of mercury atoms was accomplished by both exciting and detecting the fluorescence from the $6p\ ^3P_1^\circ - 6s^2\ ^1S_0$ transition at 253.652 nm. A narrowband interference filter centered at 250 nm was utilized to isolate the fluorescence. The rate of this reaction is slow so that we can only report an upper limit. Detection of mercury atoms could be observed only up to a temperature of 423 K in partial pressures of N_2O up to 18.6 Torr. The lifetime of mercury under these conditions was approximately 6200 μs. Various precursor molecules were tried for mercury, but a satisfactory precursor which was stable above 423 K was not found. Based on these data, we report an upper limit for the reaction of $Hg(6s^2\ ^1S_0)$ at 423 K of 5×10^{-16} molecule^{-1} cm^3 s^{-1}. Assuming a preexponential factor of approximately the gas kinetic collision rate, we can place a lower limit on the activation energy of approximately 45 kJ/mol.

Discussion

The group 11 metal atoms studied here exhibit extremely low reactivities with nitrous oxide despite their ground-state s^1 electron configurations. Two groups have previously reported on the reaction of copper with N_2O. Fontijn and co-workers[10] found an activation energy of 39.6 kJ/mol, whereas Vinckier and co-workers[14] determined an activation energy of 48.6 kJ/mol. Thus, copper was found to be only slightly reactive although copper is much more reactive with N_2O than both silver and gold. Copper's reactivity is unusual in that the 3d transition metals are generally less reactive than their 4d and 5d congeners.[33]

All of the group 12 metals are unreactive with N_2O. In a previous study, zinc was reported to react very slowly with N_2O with a reported upper limit rate constant of 1×10^{-16} molecule^{-1} cm^3 s^{-1} at 623 K.[33] Thus, the closed valence s and d subshells in these atoms renders these atoms unreactive toward abstracting an oxygen atom from N_2O.

The group 10 transition metals all exhibit pressure-dependent kinetics with N_2O. The only other transition metal to exhibit termolecular kinetics with N_2O is iridium;[26] however, iridium's limiting low-pressure third-order rate constants are almost 2 orders of magnitude smaller than the least reactive of the group 10 metals (nickel). The room-temperature limiting low-pressure third-order rate constants for ground-state Ni, Pd, and Pt are 8.2×10^{-32}, 2.5×10^{-30}, and 3.7×10^{-31} molecule^{-2} cm^6 s^{-1}, respectively.[31,33] Thus, palladium is the most reactive toward adduct-formation of the group 10 atoms. Palladium is unique among the group 10 atoms by not exhibiting an abstraction channel. Both nickel and platinum exhibited an abstraction channel with a barrier; that is, the low-pressure *second-order* rate constants increase with increasing temperature for these atoms. The lack of an s electron in the valence shell of palladium may help in adduct formation because of decreased repulsion but inhibits PdO bond formation required for the abstraction reaction. The unusually small bond energy of PdO has been attributed to the unique closed-shell structure of the palladium atom.[36]

Various mechanisms have been proposed to explain transition metal/N_2O reactions. Initial studies by Weisshaar and co-workers[8] of Sc, Ti, and V with simple oxygen-containing oxidants (including N_2O) indicated a relationship between the rate constant and the ionization energy of the transition metal and the electron affinity of the reactant. They proposed what is now termed the electron-transfer mechanism. In this mechanism, it is envisioned that as the metal atom approaches the N_2O molecule an electron from the transition metal transfers to the N_2O molecule similar to the harpoon mechanism. However, because of the relatively high ionization energies of the transition metals and the relatively low electron affinity of the N_2O, the metal$-N_2O$ distance at which the electron "jumps" is much closer than in the prototypical alkali metal/halogen reaction. Further experimental results indicated this mechanism does not adequately describe these reactions, although there does appear to be a loose connection between the ionization energies of the transition metals and the experimentally measured energy barriers (Table 2).

Another mechanism proposed to describe these reactions is the direct abstraction model.[7] This model supposes the ease with which an oxygen atom is abstracted from the N_2O is dependent upon the electron configurations of the metal atom and the metal oxide product. A large majority of the metal oxide products have one electron in the metal atom's valence s orbital, i.e., the highest occupied σ molecular orbital. In this model, the barrier to the reaction is related to the promotion energy of the ground state to the lowest lying state with a single electron in the valence s orbital. The fact that many of the transition metals with ground-state s^1 electron configurations have large energy barriers (Table 2) indicates this mechanism does not fully explain the entire transition metal series.

Fontijn and co-workers have proposed a semiempirical method to calculate energy barriers for transition metal/N_2O reactions called the SECI (semiempirical configuration interaction) model.[37,38] In SECI, the Arrhenius parameters are estimated by taking into account the ionization energy and sp promotion energy of the transition metal atom, the electron affinity of N_2O, and the bond energy of the metal oxide product. The original formulation of the model was based primarily on main group reactions and when applied to TM atoms gave inconsistent results.[37] Blue and Fontijn have formulated an improved model specifically for TMs.[38] In this formulation, the experimental activation barrier for one "basis" reaction is used to determine activation barriers for an entire series. Transition metal series based on valence electron structures gave six groups, each differing only by the contiguous number of d electrons. Table 2 lists the calculated values of the energy barriers (E_{SECI}) along with the experimentally determined activation energies. E_{SECI} is calculated based on $k(T)$ having a $T^{1/2}$ factor included in the preexponential term, so comparisons with activation energies calculated from the Arrhenius form cannot be directly made. However, the differences in the two forms result in only small variations in the calculated energies. Including a correction for the different equation forms, Blue and Fontijn report the calculations for the six TM groups yield an average deviation of $|E_{SECI} - E_{exp}|$ of only 3.8 kJ/mol,[38] although the calculated values for Ni, Mo, and Re show an alarmingly large deviation from the experimental values. Although not as general as the original formulation, the results are considerably more accurate

TABLE 2: Transition Metal Ionization Potentials and sp Promotion Energies, Transition Metal Oxide Bond Energies, Enthalpies of Reaction, and Experimental and Calculated Activation Barriers for the Reaction TM(g) + N_2O(g) → TMO(g) + N_2(g)

metal	IP[a] (kJ/mol)	sp PE[a] (kJ/mol)	TMO BE[b] (kJ/mol)	$\Delta H°$ [b] (kJ/mol)	E_{SECI}[c] (kJ/mol)	E_a(exp) (kJ/mol)	ref
Sc($s^2d^1\ ^2D_{3/2}$)	631	187	677	−514	10.4	12.0	21
Ti($s^2d^2\ ^3F_2$)	658	193	668	−501	12.4	14.3	11
V($s^2d^3\ ^4F_{3/2}$)	651	196	621	−470	12.0	10.7	33
Cr($s^1d^5\ ^7S_3$)	653	279	425	−291	[20.8]	21.1	33
						20.5	13
Mn($s^2d^5\ ^6S_{5/2}$)	717	220	399	−190	42.3	44.7	15
Fe($s^2d^6\ ^5D_4$)	762	231	386	−248	47.3	44.4	16
						49.4	17
						45.7	32
Co($s^2d^7\ ^4F_{9/2}$)	759	282	380	−214	55.1	48.8	33
Ni($s^2d^8\ ^3F_4$)	737	308	377	−215	56.5	11.3	33
Cu($s^1d^{10}\ ^2S_{1/2}$)	745	365	266	−113	[39.6]	39.6	10
						48.6	14
Zn($s^2d^{10}\ ^1S_0$)	906	387	<267	>−103	[51.7]	>65	33
Y($s^2d^1\ ^2D_{3/2}$)	600	179	715	−542	1.0	4.0	29
Zr($s^2d^2\ ^3F_2$)	640	177	772	−628	1.7	3.3	28
Nb($s^1d^4\ ^6D_{1/2}$)	652	199	765	−595	0.0	∼0	22
Mo($s^1d^5\ ^7S_3$)	684	306	556	−431	8.0	41	18
Ru($s^1d^7\ ^5F_5$)	710	302	524	−346	0.0	38	19
Rh($s^1d^8\ ^4F_{9/2}$)	720	324	401	−254	0.0	1.3	25
Pd($d^{10}\ ^1S_0$)	804	609	234[d]	−72	[>59.3]	*e*	this work
Ag($s^1d^{10}\ ^2S_{1/2}$)	731	354	217	−53	[41.3]	>60	this work
Cd($s^2d^{10}\ ^1S_0$)	868	360	∼232	∼−68	[49.3]	>80	this work
La($s^2d^{12}D_{3/2}$)	538	159	797	−634	0.0	∼0	29
Hf($s^2d^2\ ^3F_2$)	659	215	797	−651	9.5	11.3	28
Ta($s^2d^3\ ^4F_{3/2}$)	761	208	795	−672	14.8	13.6	23
W($s^2d^4\ ^5D_0$)	770	232	668	−508	19.3	25.6	24
Re($s^2d^5\ ^6S_{5/2}$)	760	227	∼623	∼−455	17.2	>50	30
Os($s^2d^6\ ^5D_4$)	843	281	∼594	∼−365	29.8	38.1	20
Ir($s^2d^7\ ^4F_{9/2}$)	873	315	410	−244	35.5	>45	26
Pt($s^1d^9\ ^3D_3$)	865	361	387	−225	[46.2]	−6[f]	31
Au($s^1d^{10}\ ^2S_{1/2}$)	890	447	219	−53	[56.4]	>70	this work
Hg($s^2d^{10}\ ^1S_0$)	1007	450	∼209	∼−90	[60.9]	>45	this work

[a] Reference 37. [b] References 3 and 4. [c] Calculated in refs 37 and 38 for an equation of the form $k(T) = AT^{1/2} \exp(-E_{SECI}/RT)$, values in brackets are from ref 37. [d] Reference 36. [e] No bimolecular component measured. [f] Calculated from the rate constants reported in ref 31.

than the original formulation. The best results are obtained by direct comparison to the measurements of a closely similar element.

Recently, two groups have attempted to use calculations to determine the energy barriers in 3d transition metal/N_2O reactions. Vinckier and co-workers[39] used density functional theory and the coupled cluster method to calculate transition state geometries and energy barriers in these reactions. The calculations were unable to quantitatively reproduce the experimental barriers, but a good correlation between the activation barrier and the binding energy of the formed transition metal oxide was found. They also found that the $3d^{n+1}s^1$ electron configuration deviated from this trend; that is, this configuration is more reactive than the $3d^ns^2$ configuration.

Recently, Stirling[40] has performed density functional calculations for the Sc→Ni reactions with N_2O. The calculations support "the electron-transfer-assisted oxygen abstraction" mechanism in which the reactions are initiated by an electron transfer from the transition metal to the N_2O molecule. This electron transfer assists the N−O bond weakening and the $O^-(^2P)$ abstraction to the metal atom without surface crossing. Charge back-donation from the N_2O to the metal follows, forming additional bonds between the reactants. Significant 4s−3d hybridization takes place on the metal atom, facilitating the electron transfer to the N_2O molecule. The result is that the reactant and product channels connect on a single potential energy surface. Thus, this mechanism exhibits the basic features of the simple electron transfer and direct abstraction mechanisms.

Table 2 lists the experimental activation energies for all of the nonradioactive transition metals reacting with N_2O. The wide range of barrier heights indicates a complex relationship between the way the reactant potential energy surfaces evolve into products. To understand the reactions of transition metal atoms with N_2O, attention must be given to multidimensional intersections among diabatic potential energy surfaces arising from both ground and low-lying excited states of the reactants. The large number of low-lying states for many transition metals means numerous potential energy surfaces are accessible in the entrance channel. Many of the reactions of transition metals with N_2O have large exothermicities so that various product channels may be accessed. Consequently, the activation barrier is a complex interplay of how a transition metal's reactant surfaces evolve into the accessible product channels. Because all transition metal/N_2O reactions require transitions from reactant surfaces of $O(^1D_2)$ character to surfaces of $O(^3P)$ character to access low-energy product states, barriers are expected unless other factors make alternative excited state channels (with possibly lower barriers) accessible. Transition metals with a large number of low-lying atomic states and a large number of low-lying excited states in their oxides are expected to increase the likelihood of a smaller barrier because alternate pathways with possible lower barriers than the ground-state reaction may become accessible. Furthermore, the greater the magnitude of the exothermicity, the more energy available to access metal oxide excited states. Thus, a reaction with a large exothermicity should improve the likelihood of a smaller barrier. Loose correlations between ionization energies, sp promotion energies, and metal oxide bond

energies have been reported. However, further understanding of the mechanisms in these reactions awaits more accurate theoretical calculations beyond the rudimentary attempts reported thus far.

Acknowledgment. Acknowledgment is made to the donors of the Petroleum Research Fund, administered by the American Chemical Society, for partial support of this research.

References and Notes

(1) Plane, J. M. C. In *Gas-Phase Metal Reactions*; Fontijn, A., Ed.; Elsevier: Amsterdam, 1992; p 29.
(2) Campbell, M. L. *J. Chem. Phys.* **1999**, *111*, 562.
(3) Chase, M. W., Jr.; Davies, C. A.; Downey, J. R., Jr.; Frurip, D. J.; McDonald, R. A.; Syverud, A. N. *J. Phys. Chem. Ref. Data* **1985**, *14*, Suppl. 1.
(4) Wagman, D. D.; Evans, W. H.; Parker, V. B.; Schumm, R. H.; Halow, I.; Bailey, S. M.; Churney, K. L.; Nuttall, R. L. The NBS tables of chemical thermodynamic properties. *J. Phys. Chem. Ref. Data* **1982**, *11*, Suppl. 2.
(5) Jonah, C. D.; Zare, R. N.; Ottinger, C. J. *J. Chem. Phys.* **1972**, *56*, 263.
(6) Raiche, G. A.; Belbruno, J. J. *Chem. Phys. Lett.* **1987**, *134*, 341.
(7) Ritter D.; Weisshaar, J. C. *J. Phys. Chem.* **1989**, *93*, 1576.
(8) Ritter, D.; Weisshaar, J. C. *J. Phys. Chem.* **1990**, *94*, 4907.
(9) Parnis, J. M.; Mitchell, S. A.; Hackett, P. A. *J. Phys. Chem.* **1990**, *94*, 8152.
(10) Narayan, A. S.; Futerko, M. P.; Fontijn, A. *J. Phys. Chem.* **1992**, *96*, 290.
(11) Campbell, M. L.; McClean, R. E. *J. Phys. Chem.* **1993**, *97*, 7942.
(12) Clemmer, D. E.; Honma, K.; Koyano, I. *J. Phys. Chem.* **1993**, *97*, 11480.
(13) Fontijn, A.; Blue, A. S.; Narayan, A. S.; Bajaj, P. N. *Combust. Sci. Technol.* **1994**, *101*, 59.
(14) Vinckier, C.; Verhaeghe, T.; Vanhees, I. *J. Chem. Soc., Faraday Trans.* **1994**, *90*, 2003.
(15) Campbell, M. L. *J. Chem. Phys.* **1996**, *104*, 7515.
(16) Campbell, M. L.; Metzger, J. R. *Chem. Phys. Lett.* **1996**, *253*, 158.
(17) Plane, J. M. C.; Rollason, R. J. *J. Chem. Soc., Faraday Trans.* **1996**, *92*, 4371.
(18) McClean, R. E.; Campbell, M. L.; Goodwin, R. H. *J. Phys. Chem.* **1996**, *100*, 7502.
(19) Campbell, M. L. *J. Chem. Soc., Faraday Trans.* **1996**, *92*, 4377.
(20) Campbell, M. L. *J. Phys. Chem.* **1996**, *100*, 19430.
(21) Campbell, M. L.; Hooper, K. L.; Kölsch, E. J. *Chem. Phys. Lett.* **1997**, *274*, 7.
(22) McClean, R. E.; Campbell, M. L.; Kölsch, E. J. *J. Phys. Chem. A* **1997**, *101*, 3348.
(23) Campbell, M. L.; Hooper, K. L. *J. Chem. Soc., Faraday Trans.* **1997**, *93*, 2139.
(24) Harter, J. S. S.; Campbell, M. L.; McClean, R. E. *Int. J. Chem. Kinet.* **1997**, *29*, 367.
(25) Matsui, R.; Senba, K.; Honma, K. *J. Phys. Chem. A* **1997**, *101*, 179.
(26) Campbell, M. L. *J. Phys. Chem. A* **1997**, *101*, 9377.
(27) Campbell, M. L. *Laser Chem.* **1998**, *17*, 219.
(28) Campbell, M. L. *J. Chem. Soc., Faraday Trans.* **1998**, *94*, 353.
(29) Campbell, M. L. *Chem. Phys. Lett.* **1998**, *294*, 339.
(30) Campbell, M. L. *J. Phys. Chem. A* **1998**, *102*, 892.
(31) Campbell, M. L. *J. Chem. Soc., Faraday Trans.* **1998**, *94*, 353.
(32) Zaslonko, I. S.; Smirnov, V. N. *Kinet. Katal.* **1998,** *39*, 485.
(33) Campbell, M. L.; Kölsch, E. J.; Hooper, K. L. *J. Phys. Chem. A* **2000**, *104*, 11147.
(34) Campbell, M. L.; McClean, R. E. *J. Chem. Soc., Faraday Trans.* **1995**, *91*, 3787.
(35) Campbell, M. L.; Plane, J. M. C. *J. Phys. Chem. A*, in press.
(36) Hildenbrand, D. L.; Lau, K. H. *Chem. Phys. Lett.* **2000**, *319*, 95.
(37) Futerko, P. M.; Fontijn, A. *J. Chem. Phys.* **1991**, *95*, 8065
(38) Blue, A. S.; Fontijn, A. *J. Chem. Phys.* **2001**, *115*, 5179.
(39) Delabie, A.; Vinckier, C.; Flock, M.; Pierloot, K. *J. Phys. Chem. A* **2001**, *105*, 5479.
(40) Stirling, A. *J. Am. Chem. Soc.* **2002**, *124*, 4058.